

Modified SH2 domain to phototrap and identify phosphotyrosine proteins from subcellular sites within cells

Akiyoshi Uezu^a, Hirokazu Okada^a, Hideji Murakoshi^{b,1}, Cosmo D. del Vescovo^c, Ryohei Yasuda^b, Dario Diviani^c, and Scott H. Soderling^{a,2}

^aDepartment of Cell Biology and ^bHoward Hughes Medical Institute and Neurobiology Department, Duke University Medical School, Durham, NC 27710; and ^cDepartment of Pharmacology and Toxicology, University of Lausanne, 1005 Lausanne, Switzerland

Edited by Tony Hunter, Salk Institute for Biological Studies, La Jolla, CA, and approved September 5, 2012 (received for review May 1, 2012)

Spatial regulation of tyrosine phosphorylation is important for many aspects of cell biology. However, phosphotyrosine accounts for less than 1% of all phosphorylated substrates, and it is typically a very transient event in vivo. These factors complicate the identification of key tyrosine kinase substrates, especially in the context of their extraordinary spatial organization. Here, we describe an approach to identify tyrosine kinase substrates based on their subcellular distribution from within cells. This method uses an unnatural amino acid-modified Src homology 2 (SH2) domain that is expressed within cells and can covalently trap phosphotyrosine proteins on exposure to light. This SH2 domain-based photoprobe was targeted to cellular structures, such as the actin cytoskeleton, mitochondria, and cellular membranes, to capture tyrosine kinase substrates unique to each cellular region. We demonstrate that RhoA, one of the proteins associated with actin, can be phosphorylated on two tyrosine residues within the switch regions, suggesting that phosphorylation of these residues might modulate RhoA signaling to the actin cytoskeleton. We conclude that expression of SH2 domains within cellular compartments that are capable of covalent phototrapping can reveal the spatial organization of tyrosine kinase substrates that are likely to be important for the regulation of subcellular structures.

protein phosphorylation | proteomics | signal transduction

One of the fundamental goals in cell biology is to identify and reveal the function of molecules in subcellular space and time to understand mechanisms of cell physiology. However, the analysis of lysates is often ineffective for the description of many subcellular proteomes. Fractionation by successive biochemical purification steps can be used to identify proteins enriched in distinct organelles, but these approaches likely alter the representation of low-abundance proteins normally associated with these organelles in their native state. Furthermore, some subcellular regions are difficult to purify biochemically. Because of the difficulty in obtaining organelle structures at high levels of purity, organelle fractionation usually requires subtractive or correlation profile analysis to identify the proteins that are enriched compared with controls (1, 2).

Reversible protein phosphorylation is a central signaling mechanism that governs important biological functions, such as migration, proliferation, differentiation, and survival. Deregulation of phosphosignaling pathways, especially tyrosine kinases, is associated with human diseases, including cancer; thus, clarifying unregulated kinase signaling pathways is one avenue toward the development of effective drug therapies and assays for these diseases (3). One of the critical yet still unresolved issues is the identity of kinase substrates and how these substrates are functionally organized within the cell to regulate physiology. Although recent advances in MS technologies have enabled the profiling of site-specific phosphorylation on a global scale (4–7), several challenges remain. These include the heterogeneity of phosphorylation sites, the discovery of low-abundance or transient phosphoproteins associated with specific cellular organelles, and

especially the identification of phosphotyrosine due to its low stoichiometry.

In vivo, phosphotyrosine can function as a ligand for docking domains. The Src homology 2 (SH2) domain is present in 111 human proteins and is the prototypic phosphotyrosine binding domain (8–11). This phosphobinding property of the SH2 domain has been used to purify tyrosine-phosphorylated proteins in vitro by affinity chromatography (12, 13). These SH2-based affinity purifications, as well as other in vitro phosphopeptide enrichment strategies, successfully identify phosphorylated proteins, although such approaches may potentially lose low-abundance or low-stoichiometric phosphotyrosine proteins during extraction. In addition, spurious phosphorylation or dephosphorylation during the lysis or purification steps likely leads to false-positive or false-negative phosphorylation sites, as well as the loss of the spatial organization of phosphoproteome.

In this study, we have taken advantage of a modified SH2 domain to develop a unique genetically encoded strategy to capture phosphotyrosine proteins in vivo in their native context at distinct subcellular sites. Using this approach, we have identified a total of 391 proteins and 189 specifically enriched proteins from each subcellular site. We further characterized one of the actin cytoskeletal enriched proteins, RhoA, and showed that it can be phosphorylated on two tyrosine residues within the switch regions.

Results

Characterization of the Site-Specific Incorporation of *p*-Benzoyl-L-Phenylalanine in c-Abl SH2. Because protein tyrosine phosphorylation status is highly dynamic in living cells, we used the SH2 domain, which has a micromolar range of binding affinity toward phosphotyrosine peptides, to capture phosphotyrosine proteins in living cells combined with an in vivo phototrapping method to trap weak and transient phosphoproteins. The photo-cross-linking amino acid *p*-benzoyl-L-phenylalanine (pBpa) can genetically incorporate into a desired site of interest within protein domains in situ by means of orthogonal tRNA/aminoacyl-tRNA synthetase pairs (Fig. 1A). We have previously used this approach to investigate actin cytoskeletal signaling mediated by Rho family GTPase Activating Protein (GAP) SH3 domain protein interaction (PI) in living cells by trapping them as they occur (14). To test the utility of the approach to identify posttranslational

Author contributions: A.U., D.D., and S.H.S. designed research; A.U., H.O., H.M., and C.D.V. performed research; R.Y. contributed new reagents/analytic tools; A.U., H.M., and D.D. analyzed data; and A.U. and S.H.S. wrote the paper.

The authors declare no conflict of interest.

This article is a PNAS Direct Submission.

¹Present address: Supportive Center for Brain Research, National Institute for Physiological Science and the Graduate University for Advanced Studies (SOKENDAI), Myodaiji, Okazaki 444-8585, Japan.

²To whom correspondence should be addressed. E-mail: scott.soderling@dm.duke.edu.

See Author Summary on page 17323 (volume 109, number 43).

This article contains supporting information online at www.pnas.org/lookup/suppl/doi:10.1073/pnas.1207358109/-DCSupplemental.

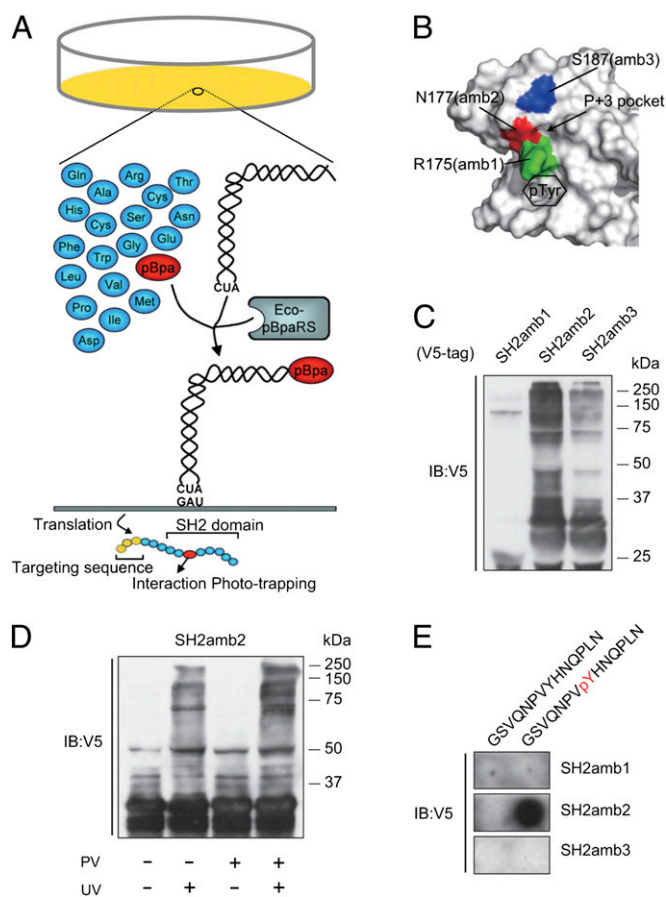


Fig. 1. SH2 domain-based in vivo phototrapping and purification of ligands. (A) Schematic of in vivo phototrapping strategy. A photoactivatable cross-linker, pBpa, is translationally incorporated into the SH2 domain, the site designated by an amber codon, when coexpressed with a pBpa-specific tRNA synthetase and amber suppressor tRNA. pBpa covalently cross-links with a binding protein on UV light exposure. (B) Positions of pBpa relative to the SH2 ligand binding pocket. The surface-rendered SH2 domain structure of c-Abl was used to determine the candidate residues (colored) to be replaced with pBpa. Phosphotyrosine and P + 3 binding pockets are indicated in the figure. (C) Estimation of phototrapping efficacy of three modified SH2 domains. Modified SH2 domains SH2amb1(R175amb), SH2amb2(N177amb), and SH2amb3(S187amb) were expressed in the cell and cultured in media containing pBpa, followed by UV exposure and purification by IgG beads. Precipitants were subjected to immunoblotting (IB) with anti-V5 antibody. (D) Photoactivation and tyrosine-dependent cross linking of SH2 domain. SH2amb2 was expressed in cells and subjected to UV light with or without PV treatment. Immunoblot analysis of purified samples by anti-V5 antibody reveals HMW bands are UV and PV treatment-dependent. (E) EGFR-derived peptides were synthesized onto cellulose membrane and overlaid with the pBpa-modified SH2 domain, followed by UV exposure, and were then immunoblotted with anti-GST antibody.

modifications, we chose the SH2 domain from c-Abl, based on previous work suggesting it recognizes large numbers of phosphotyrosine proteins (15). Three amino acid positions near the phosphotyrosyl peptide binding pocket were selected based on the crystal structure of the SH2 domain of c-Abl (16) (Fig. 1B). Each c-Abl SH2 cDNA variant containing an amber codon [SH2amb1 (R152), SH2amb2 (R175), and SH2amb3 (N177)] was cloned into the pcBpaV4 vector (14) and transfected into FreeStyle 293 cells. This pcBpaV4 vector allows for the simultaneous expression of the modified SH2, together with the pBpa-specific variant of *Escherichia coli* tyrosyl-tRNA^{Tyr} (*Eco*-pBpaRS) and the *Bacillus stearothermophilus* suppressor tRNA^{Tyr}. Also, pcBpaV4 adds affinity tags to the N terminus of the cloned insert, such that the SH2 domain can be efficiently

purified by tandem affinity purification (TAP). This vector also allows for the detection of expressed SH2 domains by a C-terminal V5 epitope. pBpa was added to the growth media for 3 d posttransfection, after which the cells were treated with pervanadate (PV), followed by exposure to 365-nm light. Purified samples from these lysates were immunoblotted to determine SH2 expression by amber codon suppression (Fig. 1C). SH2amb1 expression was consistently low, yet SH2amb2 showed intense signals with high-molecular-weight (HMW) bands compared with SH2amb3, indicating covalent binding to cellular proteins. To test whether these HMW bands were photo-cross-linking-dependent, SH2amb2 was purified with and without UV light exposure (Fig. 1D). The results showed HMW bands were UV light-dependent, indicating most of the HMW bands were endogenous proteins phototrapped by SH2amb2. The HMW band intensity increased when cells were treated with PV, indicating the phototrapping was enhanced by increasing the levels of cellular phosphotyrosine. Moreover, under the same conditions, WT SH2 domain did not cross-link to cellular proteins, confirming that pBpa was required for cross linking in situ (Fig. S1). We also assessed the capacity of these three modified SH2 domains to bind a known c-Abl SH2 ligand using the peptide overlay method (Fig. 1E). Only SH2amb2 bound to the EGF receptor (EGFR)-derived peptide (17) in a phosphodependent manner. These results suggested that the unnatural amino acid incorporated into the SH2amb2 variant did not alter the recognition specificity toward a known phosphotyrosine peptide; however, further work would be needed to demonstrate if it retained the exact binding selectivity of the WT SH2 domain. The main goal of these experiments was to exploit the SH2 domain for its phosphobinding properties rather than to identify physiological partners of c-Abl. To this end, the overlay results confirmed that the binding was phosphodependent.

Targeting Modified SH2 Domains to Subcellular Compartments. These results suggested the expression of soluble SH2amb2 (hereafter referred to as Solu-SH2) could be used to phototrap phosphotyrosine-containing proteins within cells. Next, we targeted Solu-SH2 to specific subcellular sites within the cell to bias the trapping of phosphotyrosine proteins at these locations. Three types of subcellular localization signals were fused to the N terminus of the Solu-SH2 domain to target it to F-actin, mitochondria, or cellular membranes (Fig. 2A). To confirm whether the localization signals effectively targeted the pBpa-containing SH2 to subcellular compartments, we coexpressed each SH2 domain variant with control vectors (Fig. 2B–J). Each targeted SH2 protein colocalized with control fluorescent proteins, demonstrating the pBpa SH2 variants were targeted to the desired subcellular compartment effectively, although some soluble signal was also detected. Also, we verified the presence of tyrosine-phosphorylated proteins in each subcellular structure (Fig. 2K–S). At the sites where actin-targeted EGFP or membrane-targeted enhanced yellow fluorescent protein (EYFP) was expressed, phosphotyrosine staining was observed (Fig. 2K–P). Additionally, the mitochondria-targeted EYFP demonstrated partial overlap with phosphotyrosine staining (Fig. 2Q–S). Each SH2 variant was expressed in FreeStyle 293 cells and exposed to UV light, followed by TAP, and immunoblot analysis was performed to determine the photo-cross-linked proteins. Each SH2 variant displayed a unique banding pattern (Fig. 2T), suggesting each variant captured and enriched a unique subset of phosphoproteins.

Targeted SH2 Domains Captured Unique Proteins from Subcellular Regions. Purified fractions from each of the three distinct subcellular compartments [actin-targeted SH2 (Act-SH2), mitochondria-targeted SH2 (Mito-SH2), and membrane-targeted SH2 (Mem-SH2)] and without a targeting sequence (Solu-SH2) were subjected to solution trypsin digest, and tandem MS was performed to identify captured proteins. To compare identified proteins between each SH2pBpa variant fraction, hierarchical clustering was performed (Fig. 3A). Proteins uniquely enriched in each fraction (termed PI clusters) were identified, thus removing common proteins that copurified with the baits independent of

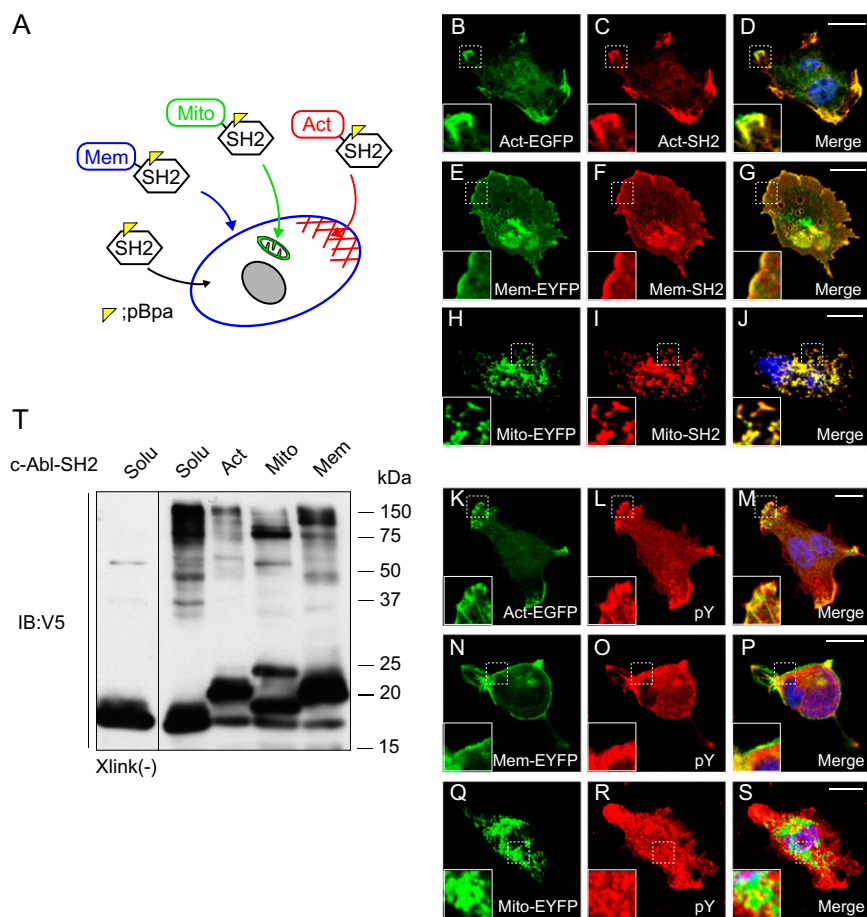


Fig. 2. Targeting modified SH2 variants to subcellular compartments. (A) Schematic diagram of strategy to target pBpa-modified SH2 domains to specific subcellular compartments within cells. (B–J) Subcellular targeting sequences (Act, F-actin; Mito, mitochondria; Mem, membrane) fused to the modified SH2 (SH2pBpa) were coexpressed with the targeting sequence fused to a fluorescence protein (EGFP or EYFP) in FreeStyle 293 cells. SH2 expression was detected by anti-V5 immunostaining. Actin-targeted EGFP (Act-EGFP) and Act-SH2 (B–D), membrane-targeted (Mem) EYFP and Mem-SH2 (E–G), and mitochondria-targeted (Mito) EYFP and Mito-SH2 (H–J) are shown. (Scale bars, 10 μ m.) (K–S) To verify the presence of phosphotyrosine proteins in each subcellular region, cells expressing targeted fluorescent proteins were immunostained with anti-phosphotyrosine antibody. Act-EGFP (K–M), Mem-EYFP (N–P), and Mito-EYFP (Q–S) are shown with corresponding images of phosphotyrosine staining. (Scale bars, 10 μ m.) (T) Purification of modified SH2 cross-linked protein complexes. Each SH2 variant was purified and subjected to immunoblotting (IB) analysis by anti V5-antibody.

their location. These could result from a low level of nontargeted SH2 due to overexpression of the tagged domain or from non-specific interactions. These PI clusters included 97 proteins from Solu-SH2, 46 proteins from Act-SH2, 24 proteins from Mito-SH2, and 22 proteins from Mem-SH2 (Dataset S1). The proteins within each PI cluster were heavily enriched for the subcellular region targeted by the SH2pBpa variants. For example, Act-SH2 phototrapping identified proteins known to be regulators of or localized to actin, including RhoA, myosin VI, gelsolin, LIMA1, and IQGAP1. By comparative analysis with the PhosphoSite and Phospho.ELM databases, potentially unique phosphoproteins were identified in each enrichment fraction (Fig. S2), indicating the targeting and phototrapping approach could capture unique potential phosphotyrosine proteins from subcellular compartments. In addition, BCAR1, which is known to interact with c-Abl in an SH2-dependent manner, was captured in the soluble, actin, and mitochondria fractions (18). Thus, consistent with our EGFR peptide overlay, these data indicate the pBpa-containing SH2 domain retains its natural binding selectivity. Importantly, in each subcellular-targeted SH2 PI cluster, the portion of the target subcellular localization predicted by gene ontology for the identified proteins was increased compared with the Solu-SH2 PI cluster (Fig. 3B). These results further demonstrate that targeting SH2 domain to each subcellular compartment biased the phototrapping of phosphoproteins that naturally occur at that subcellular region in situ.

Identification of Potential SH2 Binding Phosphorylation Sites by Peptide Array Overlay. It is likely that in addition to phosphorylated proteins, nonphosphorylated proteins associated with the SH2 binding proteins would be present in the purified samples. To identify the potential tyrosine-phosphorylated proteins and the sites on these proteins that could serve as the SH2 docking site, we performed peptide array analysis. Sequences surround-

ing tyrosine sites from a sample of the most abundant proteins (based on peptide spectral counts) that were found in each SH2 PI cluster were arrayed onto membranes as phosphotyrosine and nonphosphotyrosine peptides. These arrays were then incubated with GST c-Abl SH2 domain, and bound GST-SH2 was detected by immunoblotting. A total of 182 peptides from 25 proteins were analyzed (Dataset S2). The resulting intensity for binding at each peptide, nonphosphopeptide vs. phosphopeptide, was measured and normalized to a positive control peptide derived from EGFR. For example H-Ras harbors nine potential phosphotyrosine sites, one of which (Y157) was reported in a phosphoproteomic study to be phosphorylated (19). Overlay analysis confirmed the Y157 could function as an SH2 binding site in addition to other potential phosphotyrosine sites, such as Y32 (Fig. 4A and B). Representative results from parallel anti-phosphotyrosine blotting and GST-SH2 overlays verified that negative binding results were not due to variability in the phosphotyrosine peptide synthesis (Fig. S3), consistent with other studies demonstrating the highly reproducible nature of phosphotyrosine peptide array synthesis and SH2 domain overlay (20). Of a total 182 peptides, 28 were previously identified as phosphorylated (Fig. 4B). The SH2 overlay screening identified 10 of these peptides. Additionally, 49 previously undescribed potential SH2-binding phosphorylation sites were identified. Binding sequences identified from the peptide array were aligned to deduce the preferred c-Abl SH2 binding sequence flanking the phosphotyrosine site (Fig. 4C). Previously the c-Abl SH2 domain was reported to show selectivity for a common pY[–][–] ϕ motif, where [–] and ϕ designate negatively charged and hydrophobic residues, respectively (21). The binding data obtained here are consistent with this specificity, although the c-Abl SH2 domain has shown a broader binding spectrum, which, in turn, makes it useful for trapping phosphotyrosine peptides in vivo.

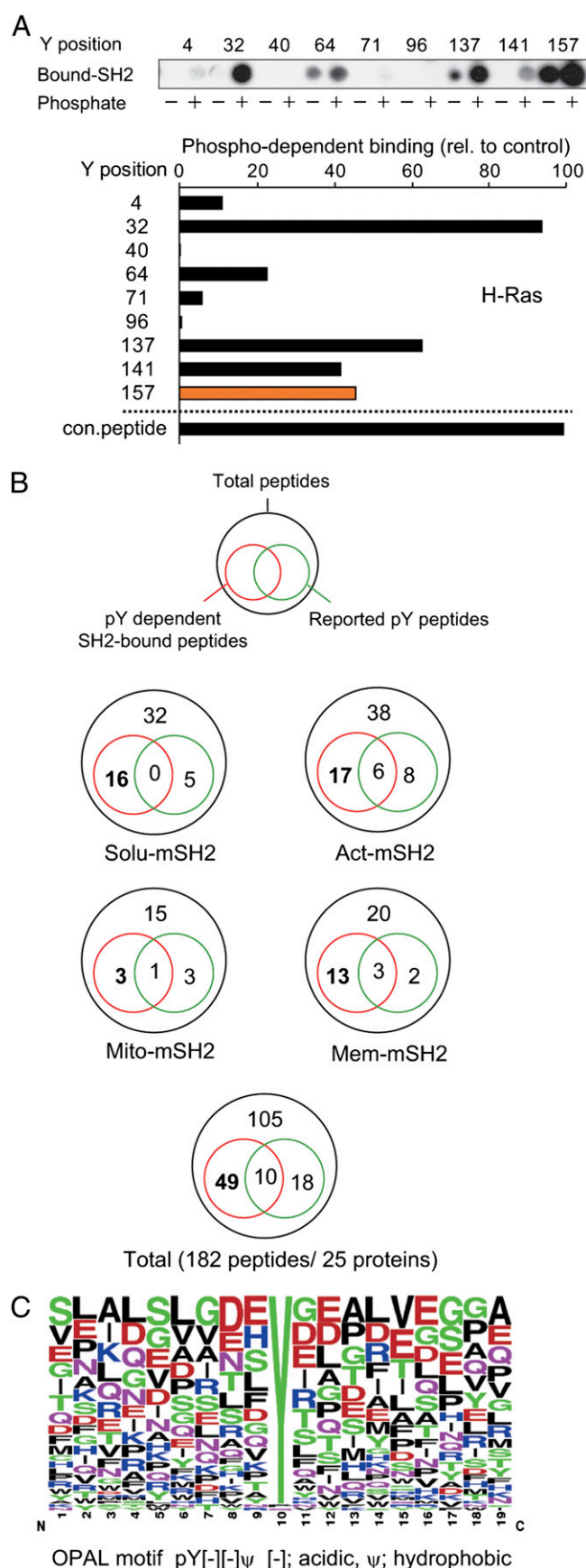


Fig. 4. Phosphotyrosine binding profile of targeted SH2 binding proteins. (A) Peptide array-based in vitro SH2 binding profile. Peptides surrounding

could be phosphorylated (19). Interestingly, endogenous RhoA phosphorylation was detected only when coexpressed with Bcr-Abl in the presence of PV, indicating the phosphorylation of RhoA may be tightly regulated by phosphatase activity (Fig. 5E). To map the responsible phosphorylation site in situ, mutagenesis analyses were performed (Fig. 5F). Y34F and Y66F RhoA mutants reduced tyrosine phosphorylation levels to 50% and 20%, respectively, compared with controls when they were coexpressed with Src (Fig. 5G). When these RhoA mutants were coexpressed with Bcr-Abl, phosphorylation levels of Y34F and Y66F RhoA mutants dramatically decreased to 32% and 17%, respectively. As expected, when Y34 and Y66 were both mutated to phenylalanine, phosphorylation was completely abolished. Together, these observations indicate that Y34 and Y66 are the two predominant phosphorylation sites, and that the Src kinase and Bcr-Abl are the two candidate kinases that may phosphorylate these sites.

Tyrosine 34 and 66 of RhoA Appear to Be Critical for Effector Binding.

Based on their location within the switch regions, one potential functional role of phosphorylation of RhoA at Y34 and Y66 could be to regulate effector binding in vivo. To investigate this possibility, the activity of RhoA vs. RhoA mutants was tested using a two-photon excitation laser scanning microscopy with fluorescence lifetime imaging (2pFLIM) assay for RhoA effector [Rho binding domain (RBD)] binding (Fig. 6A). Fluorescence lifetime decay curves of mEGFP-RhoA were measured to calculate the binding fraction of RhoA (25, 26). Constitutively active RhoA (RhoAQ63L) had an approximately twofold higher fraction of RBD binding compared with WT RhoA (Fig. 6B). To test the potential role of phosphorylation, tyrosine 34 and 66 were mutated to glutamic acid. Although acidic amino acids cannot perfectly mimic phosphotyrosine, they are the only substitutions that have successfully been used to approximate tyrosine phosphorylation in regulating protein activity (27, 28). In contrast to active RhoA, RhoAQ63L(Y34,66E) had a dramatic decrease in RBD binding. This binding fraction was even lower than that of WT RhoA, suggesting phosphorylation at these sites could have a negative effect on RhoA activity (Fig. 6B). To test this notion further, RhoAQ63L was coexpressed with constitutively active Src (SrcCA) or dominant negative Src (SrcDN) (Fig. S5A). SrcCA reduced the binding of RhoAQ63L (17.4%) compared with SrcDN (Fig. 6C). Because the glutamine 63 to leucine mutation in the switch 2 region of GTPases both increases basal GDP/GTP exchange and inhibits intrinsic GTPase activity, the RhoAQ63L is relatively insensitive to the activity of cellular GAPs and GEFs (29–31). Thus, the effect of Src was a likely a direct effect on the sensor. This effect was likely via Src phosphorylation of RhoA vs. the RBD domain of the sensor because control experiments demonstrated that although Src could phosphorylate RhoA, it could not phosphorylate the RBD domain (Fig. S5B). Together, these data suggest Y34 and Y66 are critical for the ability of RhoA to interact with downstream effectors on activation and that phosphorylation at these sites would likely inhibit activation-dependent effector binding. This possibility was tested using WT RhoA vs. RhoA(Y34,66E) in a RhoA activation assay in response to EGF treatment (Fig. 6D). RhoA(Y34,66E), WT RhoA, and dominant negative RhoA (RhoAT19N) were expressed in the cells and stimulated with EGF to induce activation (32). As expected, WT RhoA was potently

tyrosine sites within H-Ras, which was found in the membrane-targeted SH2 PI cluster, were synthesized on cellulose membrane, followed by incubation with GST-SH2, and were immunoblotted with anti-GST antibody. Relative binding strength was estimated by subtracting the intensity of phosphopeptide from that of nonphosphopeptide and normalized to the control peptide derived from EGFR. The colored bar indicates a previously reported phosphorylation site (19). con., control. (B) Summary of peptide array binding assay. A Venn diagram of each targeted SH2 PI cluster represents the composition of identified phosphotyrosine-dependent peptides and the reported phosphorylated tyrosine sites. (C) Motif analysis of c-Abl SH2 binding sites. OPAL, Oriented Peptide Array Library.

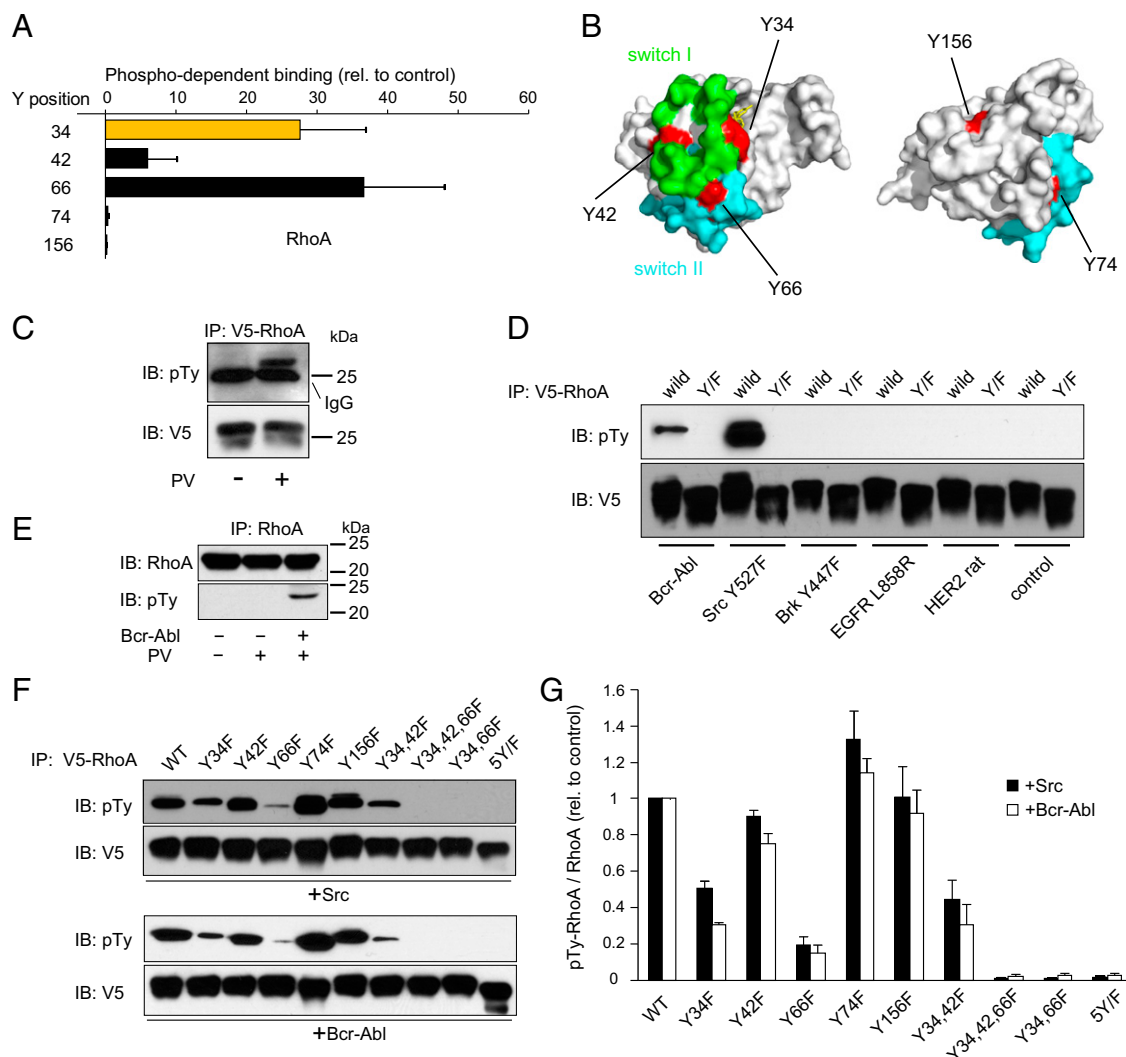


Fig. 5. Phosphotyrosine profile of RhoA. (A) Peptides derived from RhoA were synthesized on cellulose membrane, followed by incubation with GST-SH2, and were immunoblotted with anti-GST antibody. Relative binding strength is shown. Bars represent mean \pm SEM ($n = 3$). (B) Surface representations of the structure of RhoA with switch I and II regions (green and blue, respectively) and five tyrosine sites (red). (C) RhoA is tyrosine-phosphorylated. V5-tagged RhoA was expressed in 293T cells and treated with or without PV. After lysis, RhoA was immunoprecipitated (IP) by V5 antibody and immunoblotted (IB) with antiphosphotyrosine antibody. (D) Candidate screen of potential RhoA tyrosine kinases. V5-tagged WT RhoA or RhoA with all tyrosines substituted to phenylalanine was coexpressed with the indicated kinases in 293T cells. Immunoprecipitated samples were blotted with antiphosphotyrosine antibody. (E) RhoA is tyrosine-phosphorylated in vivo. Endogenous RhoA was immunoprecipitated from 293T cells transfected with or without Bcr-Abl and treated with PV. Precipitates were immunoblotted with anti-RhoA antibody (*Upper*) or with antiphosphotyrosine antibody (pTy; *Lower*). (F) RhoA is tyrosine-phosphorylated on tyrosines 34 and 66. Various RhoA mutants were coexpressed with Src or Bcr-Abl and treated with PV, followed by immunoprecipitation with anti-V5 antibody. Precipitates were blotted with antiphosphotyrosine antibody (*Upper*) or anti-V5 antibody (*Lower*). (G) Quantitative analysis of tyrosine-phosphorylated RhoA mutants was obtained by densitometry. The amount of phospho-RhoA was normalized to the amount of precipitated RhoA. rel., relative. Bars represent mean \pm SEM ($n = 3$).

activated by EGF treatment. In contrast, RhoA(Y34,66E) was not responsive and behaved similar to RhoAT19N (Fig. 6 *D* and *E*).

Role of Y34 and Y66 of RhoA in Effector Binding and RhoA-Induced Actin Stress Fiber Formation. These results suggested phosphorylation of RhoA at Y34 and Y66 may inhibit binding to cellular effectors. To test this possibility, GFP-tagged RhoAQ63L or its mutant, RhoAQ63L(Y34,66E), expressed in cells was immunoprecipitated to compare interacting partners (Fig. 7A). MS-based comparative analysis of the immunoprecipitates showed that RhoA effectors involved in the regulation of the actin cytoskeleton, such as DIAPH1, DAAM1, ROCK1/2, and PKN, were detected only in the RhoAQ63L immunoprecipitations (Fig. 7B). Also, Rhotekin, which was used as an effector binding for 2pFLIM assay, was associated with RhoAQ63L but not with RhoAQ63L

(34,66E). Importantly, RhoGAP1, a GTPase activating protein for RhoA and Cdc42 (33, 34), was associated with both RhoA mutants, suggesting that altering tyrosine 34 and 66 does not disrupt this binding. These observations indicate that Y34 and Y66 are critical for effector binding but not for GAP binding. Importantly, it also shows the mutations did not globally disrupt RhoA folding or function but did selectively impair its ability to bind effectors. To determine the role of each tyrosine with regard to effector binding, an RBD pull-down assay was performed (Fig. 7 C and D). Both Y34 and Y66 were critical for Rhotekin binding, suggesting phosphorylation of either site could inhibit RhoA effector functions.

Based on these results, the functional consequences to RhoA-induced cellular actin reorganization were assessed (Fig. 7*E* and *F*). For this assay, RhoA (wild), RhoAQ63L, and mutants of

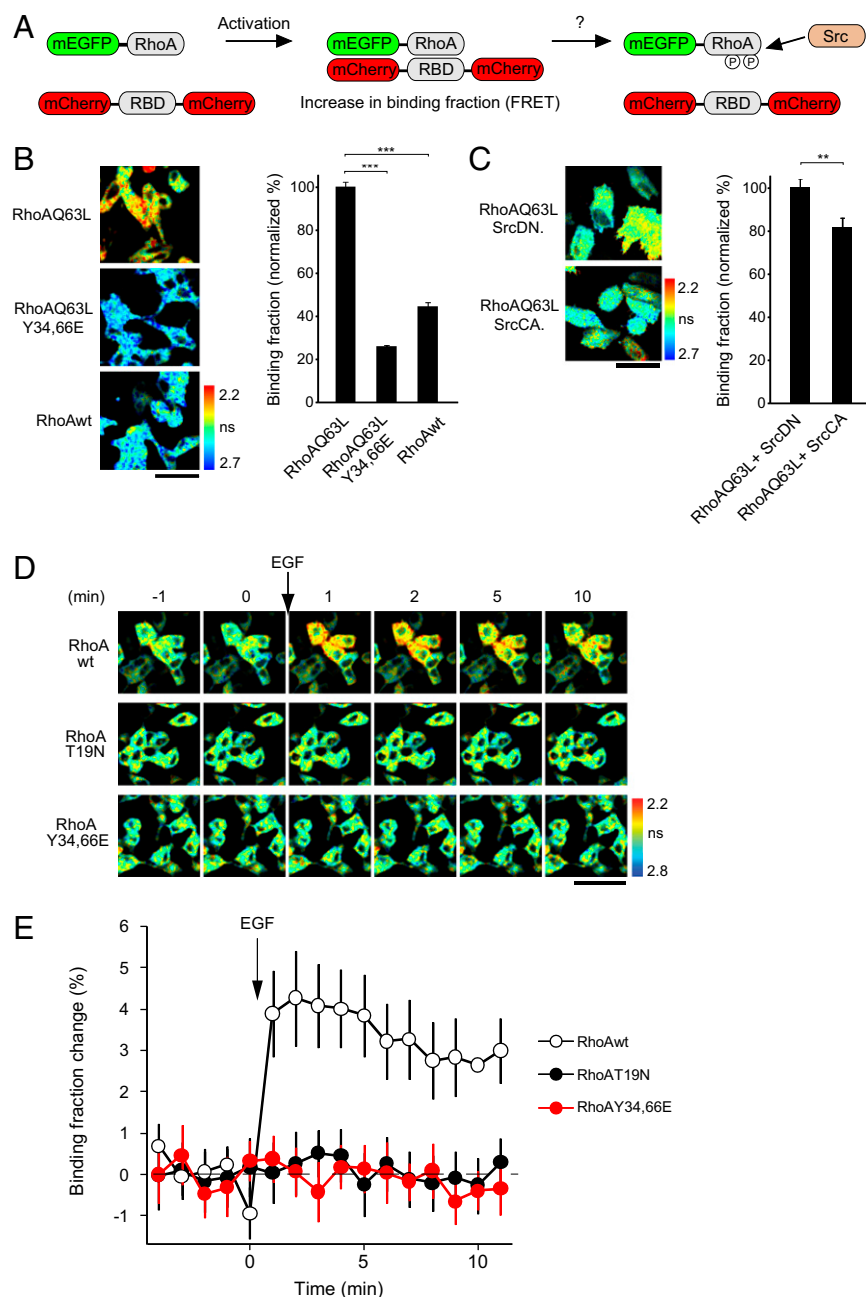


Fig. 6. Tyrosines 34 and 66 of RhoA are crucial for effector binding in cells. (A) Schematic of the RhoA activity FRET sensor. mEGFP was tagged to the N terminus of RhoA, and mCherry was attached to the N and C termini of the RBD of Rhotekin (8–89 amino acids). When RhoA is activated, RBD binds to RhoA, producing FRET between mEGFP and mCherry. (B) (Left) Representative fluorescence lifetime images in HeLa cells. Cells were transfected with dominant active RhoA (RhoAQ63L), dominant active phosphomimic mutant with both tyrosines 34 and 66 substituted to glutamic acid [RhoAQ63L(Y34,66E)], and WT RhoA (RhoAwt). Warmer colors indicate shorter lifetimes and higher levels of RhoA activity. (Right) Relative binding fraction of RhoA mutants. Bars represent mean \pm SEM ($n \geq 10$). *** $P < 0.001$. (C) (Left) Representative fluorescence lifetime images in HeLa cells of RhoAQ63L coexpressing SrcDN or SrcCA. (Right) Relative binding fractions of RhoAQ63L. Bars represent mean \pm SEM ($n \geq 50$) from three independent experiments. ** $P < 0.01$. (D) Fluorescence lifetime images of RhoA activation induced by EGF. WT, phosphomimic mutant (Y34,66E), or dominant negative (T17N) RhoA was expressed in HeLa cells and stimulated with 20 nM EGF, and activity was measured by 2pFLIM. (E) Graph depicts the time course of RhoA activation indicated by the change in the fraction of RhoA bound to the sensor. Bars represent mean \pm SEM. (Scale bars, 50 μ m.)

RhoAQ63L containing either phenylalanine or glutamic acid at positions Y34 and Y66 were overexpressed in serum-starved HeLa cells and the percentage of transfected cells with elevated actin stress fiber formation was quantified. As expected, RhoAQ63L strongly induced actin stress fibers in HeLa cells, almost sixfold that of WT RhoA, which weakly stimulated stress fiber formation. In contrast, the RhoAQ63L(Y34,66E) mutant completely lost the ability to induce F-actin formation, whereas RhoAQ63L(Y34,66F) retained significant activity. These data indicate the difference in ability to stimulate cellular stress fiber formation is due to the negative charge of glutamic acid compared with the structurally similar phenylalanine. Interestingly, these results almost perfectly mirror the effector binding results of Fig. 6B, which also showed the Y34,66E form of RhoA is less active than WT RhoA.

Discussion

Here, we have demonstrated the utility of unnatural amino acid-based photo-cross linking to identify transient posttranslational

modifications in vivo. Importantly, we were able to use this approach in combination with a relatively low-affinity PI module, the SH2 domain, to trap and identify transient phosphorylation events that occur at low stoichiometry. We also show this approach can be extended to interrogate phosphorylation events within distinct subcellular sites. This method should be applicable to other PI modules and opens up new avenues for exploring the organization of posttranslational modifications in cellular space.

For the initial testing of this approach, we focused on the SH2 domain. SH2 domains are particularly well suited as cellular phosphotyrosine probes in that they protect these sites from rapid dephosphorylation in vivo. However, the intrinsic low binding affinity has limited their utility for purification of their cellular ligands. This limitation was overcome by the translational incorporation of the photo-cross-linkable unnatural amino acid pBpa within proximity of the ligand binding site. The evolutionary expansion of the SH2 domain to over 100 different

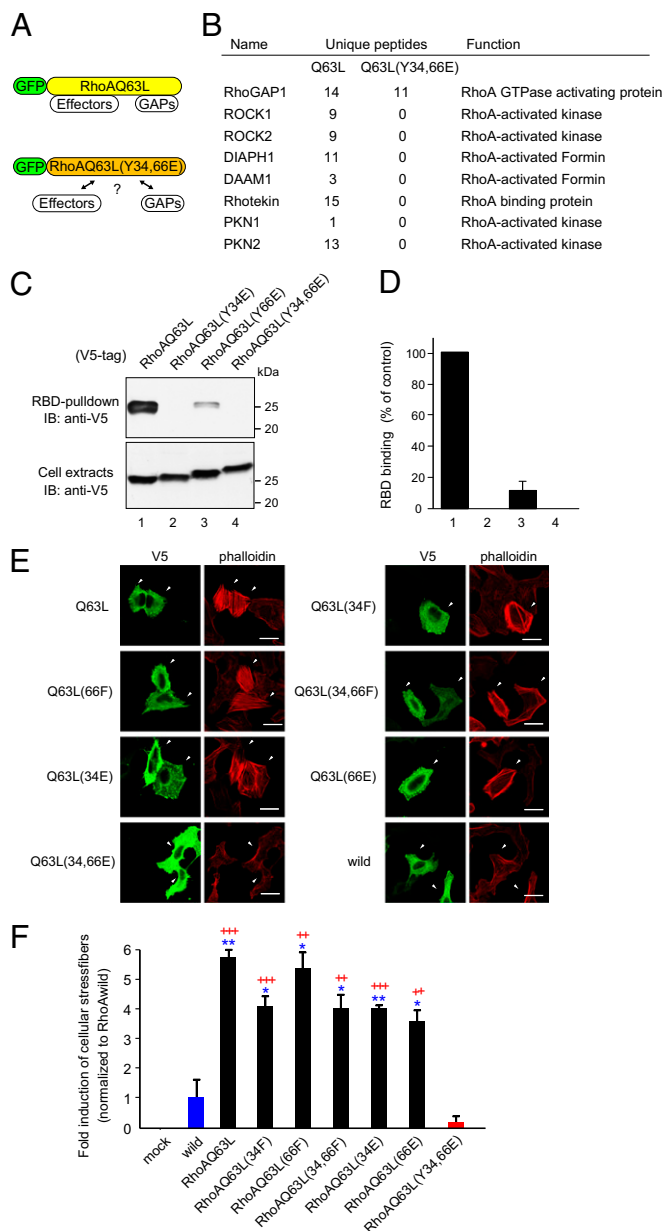


Fig. 7. Y34,66E of RhoA abolishes effector binding and stress fiber formation. (A) Schematic figures depict RhoA mutants used to identify endogenous GAPs or effectors. Constitutively active RhoA (RhoAQ63L) and its phosphomimetic (Y34,66E) mutant were tagged with GFP and expressed in 293T cells, followed by immunoprecipitation. Precipitated samples were subjected to MS analyses. (B) Identified proteins in each sample. Actin cytoskeleton-related proteins identified in constitutively active RhoA (Q63L) or RhoAQ63L phosphomimetic mutant are shown with the number of uniquely identified peptides in each protein. (C) Representative Western blot of Rho-kinase RBD pull-down assays from cells expressing RhoAQ63L or individual phosphomimetic mutants (indicated above). IB, immunoblotting. (Upper) Amounts of each RhoA mutant precipitated by the RBD pull-down are shown. (Lower) Equal levels of expression of each mutant in the lysates are shown. (D) Graph depicts the quantification of the RBD pull-downs as shown in C. Bars represent mean \pm SEM ($n = 3$). (E) Induction of F-actin stress fiber formation by RhoA mutants. V5-tagged WT RhoA (wild), constitutive active RhoAQ63L (Q63L), phosphomimetic forms of RhoAQ63L (34E, 66E, or 34,66E), or controls (34F, 66F, or 34,66F) were expressed in HeLa cells, followed by immunostaining with anti-V5 antibody and phalloidin and DAPI labeling. (Scale bars, 10 μ m.) (F) Quantitative analysis of RhoA-induced F-actin stress fiber formation. The average fluorescence intensity of F-actin in each V5-RhoA mutant-expressing cell was measured. The fold induction of cellular stress fiber formation was calculated, normalized to RhoA. Bars represent mean \pm SEM from three independent experiments.

functional variants in humans infers it is a highly robust structural scaffold capable maintaining phosphotyrosine binding in the face of mutational pressure. We exploited this property to expand the physiochemical repertoire of this domain with the incorporation of the unnatural phenylalanine analog. Because pBpa is translationally incorporated *in vivo*, this also presented the opportunity to add subcellular tags to the recombinant protein to direct the photo-cross-linking events to defined cellular sites. The advantage of this approach is that it allows the biochemical probing of subcellular sites in their native state without the need for extensive subcellular fractionation. Furthermore, it may allow for the interrogation of cellular sites not previously amenable to biochemical purification. For the initial testing of this approach, we sampled the actin cytoskeleton, mitochondria, and cellular membranes using the c-Abl SH2 domain. Our primary goal was not to identify physiological partners of c-Abl, *per se*; rather, we used this domain because previous studies had suggested it could sample a large number of phosphorylated proteins when overexpressed (15). Indeed, in each case, we were significantly able to enrich the photo-cross-linking reaction toward proteins known to exist in each of the targeted sites within cells and to be phosphorylated. In the case of the mitochondria, the SH2 domain was targeted to the intramitochondrial space, where Src family kinases have previously been localized (35). Approximately 40% of the proteins identified in the mitochondrial targeting experiments have previously been identified as phosphotyrosine substrates (Fig. S2), further confirming this cellular site can be regulated by tyrosine kinases. Additionally, many of proteins identified are likely be phosphorylated at the cellular sites the SH2 was targeted to. For example, membrane-targeted SH2 identified the multipass membrane protein ATP1A1, a Na^+/K^+ exchange pump whose activity is regulated by phosphorylation of tyrosine residue 10 (36). Indeed, this site was also identified in the peptide array as the best binding site for the Abl SH2 domain (Dataset S2). Thus, this method can be used to probe defined subcellular spaces, even within organelles in living cells.

In this study, we also attempted to identify phosphotyrosine proteins associated with the actin cytoskeleton directly. This was important, given the known effects of tyrosine kinases on important actin-driven processes, such as adhesion and migration. Our analysis identified several important regulators of actin as potential phosphotyrosine proteins, including the small GTPase RhoA. Importantly, both recombinant RhoA and endogenous RhoA were tyrosine-phosphorylated; however, interestingly, the phosphorylation was only apparent on PV treatment to inhibit phosphatase activity. These results highlight that although RhoA may be a tyrosine kinase substrate, its phosphorylation is likely to be tightly regulated in vivo or that a small fraction of total cellular RhoA is phosphorylated. Often, low stoichiometry of phosphorylation is interpreted to indicate that the likely importance of phosphorylation is questionable. However, in this case, our approach was specifically designed to identify subcellular pools of phosphorylated proteins. The phototrapping data indicated RhoA was only phosphorylated when associated with F-actin; thus, it is possible that the observed low stoichiometry is a reflection of a distinct cellular pool of total RhoA that is phosphoregulated. Further work is needed to distinguish among all these possibilities. Two key phosphotyrosine binding sites, Y34 and Y66, were identified by peptide array-based SH2 overlay analysis, and these sites were confirmed as potential phosphorylation sites by mutagenesis. Using an unrelated global phosphoproteomic approach, RhoA Y34 was also recently detected in the cancer cell line H1703 (19), further confirming this site as a likely tyrosine kinase substrate. We also screened several tyrosine kinases to determine which, if any, could target RhoA. From this screen, Src emerged as the best candidate, followed by Abl, which contains an F-actin binding domain (37). Further

dependent experiments ($n \geq 30$). *** $P < 0.001$; ** $P < 0.01$ in blue are mutants compared with RhoA. +++ $P < 0.0001$; ++ $P < 0.01$ in red are mutants compared with RhoAQ63L(Y34,66E).

work is required to identify conclusively the physiological tyrosine kinases that target RhoA; however, we note evidence in supplementary material of an article by Moritz et al. (19) that Gleevec, an Abl inhibitor, reduces the level of cellular RhoA Y34 phosphorylation. Previous reports have also shown that Src may, in fact, associate with RhoA and that Src phosphorylation can inhibit RhoA signaling, in part by phosphorylating and activating p190RhoGAP during integrin engagement (38–40). Our data suggest there could be an additional, direct inhibitory effect of Src on a subfraction of RhoA as a result of phosphorylation of Y34 and Y66. Further work is required to demonstrate that tyrosine phosphorylation of endogenous RhoA is inhibitory.

Several RhoA structures in complex with effectors and modulators have been solved, and these structures indicate Y34 and Y66 are located in important positions for multiple RhoA protein–protein contacts. For example, the structure of RhoA-GTP in complex with the ROCK RBD revealed that Y66 is in the switch II region and is involved in both electrostatic and hydrophobic interactions with ROCK1 (41). Also, Y66 is involved in the binding interaction with the HR1a domain of protein kinase C-related kinase 1, suggesting Y66 is critical for RhoA interactions with multiple types of effector binding domains (42). Additionally, structural analysis of leukemia-associated RhoGEF in complex with RhoA revealed that Y34 is involved in the interaction (43). Y34 is also critical for the activation of RhoA by the GEF AKAP-Lbc (44). Indeed, the Y34 mutant of RhoA (RhoAY34E) abolished binding with AKAP-Lbc (Fig. S6). These studies suggest phosphorylation on tyrosine 34 or 66 may yield distinct outcomes toward different classes of RhoA binding partners, yet the net outcome appears to be inhibition of RhoA-mediated signaling to the actin cytoskeleton. Consistent with a potential regulatory function for Y34, another inhibitory modification has been identified, the AMPlation of Y34, catalyzed by Fic domain-containing proteins, which can also disrupt RhoA signaling (45).

Interestingly, Y34 and Y66 are well conserved in Rho proteins, as well as in other small G-protein families (Fig. S7). Consistent with this, we also identified H-Ras as a phosphotyrosine protein in the membrane-enriched PI cluster, and our SH2 overlay mapping identified the homologous tyrosines 32 and 64 as possible sites of phosphorylation-dependent binding (Figs. 3 and 4). Additionally, Rac1, RalA, and Rab11a contain homologous tyrosine sites that have been reported to be phosphorylated (46, 19). Furthermore, Y64 of Cdc42 (corresponding to the Y66 of RhoA) is also phosphorylated by Src after EGF stimulation, and this enhances the interaction between Cdc42 and RhoGDP dissociation inhibitor (47). Recently, Rac1 was shown to be phosphorylated on Y64 by Src and FAK *in vitro* (48). Thus, the emerging data suggest that sites homologous to RhoA Y34 and Y66 in other small G proteins may function as previously undescribed phosphoregulatory sites targeted by tyrosine kinases to regulate cellular functions governed by different GTPase families.

In summary, this work describes a unique genetically encoded approach to discover phosphotyrosine proteins within the context of their spatial organization within the cell. This approach is based on the incorporation of the photoinducible cross-linking phenylalanine analog pBpa into the phosphotyrosine binding SH2 domain. Analysis of the identified proteins from each subcellular target confirms the overall approach successfully traps and enriches proteins from these defined compartments. Furthermore, this approach reveals unique targets for tyrosine kinases in different subcellular compartments that could be important for regulation. Additional analysis with SH2 domains with different binding specificities compared with Abl will likely expand the coverage of tyrosine kinase substrates within these subcellular sites.

Materials and Methods

Plasmids. A mammalian expression vector that coexpresses Eco-pBpaRS and *B. stearothermophilus* suppressor tRNA^{Tyr} (a gift from Shigeyuki Yokoyama, University of Tokyo, Tokyo, Japan) was modified for TAP (14). A strep-tag, followed by a calmodulin binding peptide (CBP), a V5 epitope, two tobacco etch virus protease cleavage sites, an HRV3C cleavage site, and a tandem protein A sequence, was inserted after a mammalian expression promoter. Unique RsrII and SbfI restriction sites were placed between the CBP and

V5 epitope for subcloning SH2 domain coding sequences. The SH2 domain (aa 120–220, Uniprot P00519) derived from c-Abl was inserted, and the targeted sequences listed below were placed on the N terminus of SH2. Lifeact, MGVDLIKKFESISKEE (49); membrane (Mem), MLCMRRTKQVEKNDEDQKI (50) (derived from neuromodulin); and mitochondria (Mito), MSVLTPLLRLGLTGSARRLPVPRAKIHL (51) (derived from cytochrome c oxidase subunit 8A) were used. The Lifeact was a gift from Michel Bagnat (Duke University). Other plasmids used in this study are detailed in *SI Materials and Methods*.

Photo-Cross Linking. Photo-cross linking was performed as described (14). Briefly, on the day of transfection, a 1-L culture of FreeStyle 293 cells was grown in FreeStyle 293 medium (GIBCO) to a density of 1×10^6 cells/mL. Transfection was done following a modified polyethylenimine (PEI) protocol (52). One milligram of the vector encoding TAP-tagged SH2 domain plus Eco-pBpaRS and suppressor tRNA^{Tyr} was mixed with 2 mg of PEI in 50 mL of FreeStyle 293 medium and added to the cell culture after 10 min of incubation. pBpa (270 mg) was dissolved in 1.1 mL of 1 M NaOH and added to the cell culture following addition of 7.5 mL of 1 M Hepes buffer to the culture. After 3 d of incubation at 37 °C, the cells were treated with 0.5 mM PV for 5 min, followed by exposure to UV light (365 nm) in a custom-built chamber. After 30 min of photo-cross linking in the chamber at 4 °C, cells were collected by centrifugation and subjected to TAP purification. Detailed methods for TAP purification can be found in *SI Materials and Methods*.

MS. MS was carried out as previously described (14). Briefly, all MS data were acquired on an LTQ-Orbitrap XL mass spectrometer (Thermo Scientific) operating in positive-ion mode with an electrospray voltage of 2.0 kV. The instrument was set to acquire a precursor MS scan in the Orbitrap XL mass spectrometer from *m/z* 40–2,000, with *r* = 60,000 at *m/z* 400 and a target automatic gain control setting of 1e6 ions. In a data-dependent mode of acquisition, tandem MS spectra of the five most abundant precursor ions were acquired in the Orbitrap XL mass spectrometer at *r* = 7,500 at *m/z* 400 with a target AGC setting of 2e5 ions. Maximum fill times were set to 1,000 ms for full MS scans and to 500 ms for tandem MS scans with minimum tandem MS triggering thresholds of 5,000 counts. For all experiments, fragmentation occurred in the LTQ linear ion trap, Finnigan LTQ (Thermo Electron Corporation), with a collision-induced dissociation energy setting of 35%, and a dynamic exclusion of 60 s was used for previously fragmented precursor ions. Details of qualitative identifications from raw liquid chromatography/tandem MS data can be found in *SI Materials and Methods*.

Hierarchical Clustering. Relative protein abundance in the sample prepared by TAP was quantified using spectral counting (53). To normalize the relative protein abundance, the spectral counts were expressed as a percentage of the total spectra observed in the sample. Mean normalized spectral counts were obtained from multiple independent experiments (*n* ≥ 2 for each targeted SH2 domain). Hierarchical clustering was performed based on the uncentered Pearson correlation of the mean normalized spectral counts (54, 55).

Peptide Array Synthesis and GST or GST-SH2amb Protein Overlay. Peptides (19mer) were synthesized as previously described (56) using Auto-Spot Robot ASP 222 (INTAVIS AG). The GST-SH2 domain was purified as previously described (57). The peptide arrays were incubated with the GST-SH2 domain at a concentration of 100 nM in 5% (wt/vol) BSA for 2 h. After a wash with Tris-buffered saline/Tween-20, the GST fusion proteins were detected using HRP-conjugated anti-GST antibody (BETHYL). Positive peptide spots were densitometrically quantified using ImageJ (National Institutes of Health). Phosphodependent binding strength was estimated by subtracting the intensity of phosphopeptide from nonphosphopeptide and then normalized to the control peptide. A peptide showing a binding strength over 20 was assessed as a phosphotyrosine-dependent SH2 binding peptide. Amber codon-modified SH2 proteins were purified by TAP purification and incubated with the peptide arrays derived from EGFR, followed by UV exposure, and banded SH2 was detected with anti-V5 antibody.

Immunoprecipitation Experiments. Immunoprecipitation experiments using HEK 293T cells were performed as previously described (58). Briefly, transfected cells were lysed and centrifuged, and the supernatant was incubated with V5 antibody-agarose (Sigma) or GFP trap-agarose (ChromoTek). After beads were washed with lysis buffer, sample buffer was added and subjected to immunoblotting. For endogenous RhoA precipitation, cells were lysed with radioimmunoprecipitation assay buffer, followed by sonication, and centrifuged, and the supernatant was incubated with agarose-conjugated anti-RhoA (26C4; Santa Cruz Biotechnology). Further details can be found in *SI Materials and Methods*.

Cell Preparation and Image Analysis. Transfected FreeStyle 293 cells were plated onto poly-D-lysine-coated coverslips, fixed, and stained with anti-V5 antibody (1:500; Invitrogen) or antiphosphotyrosine antibody (1:100, 4G10; Millipore). Images were taken on a Zeiss LSM 710 laser scanning confocal microscope with a 63×/1.4 N.A. oil-immersion objective or 20×/0.8 N.A. objective. Further details for quantification of phalloidin staining are provided in *SI Materials and Methods*.

2pFLIM Assay. Details of the 2pFLIM assay have been described previously (26). mEGFP was excited with a Ti:sapphire laser (Mai Tai; Spectraphysics) tuned at a wavelength of 920 nm. Fluorescent images were collected using a 60×/0.9 N.A. objective (Olympus). For fluorescence lifetime imaging, a photoelectron multiplier tube with low transfer time spread (H7422-40p; Hamamatsu) was used. Fluorescence lifetime images were obtained using a time-correlated single-photon counting board (SPC-140; Becker and Hickl) controlled with

custom software based on Scanimage software (open source software, Karel Svoboda, Janelia Farm, Ashburn, VA).

Statistical Tests. Statistical analysis was done using Excel 2007 (Microsoft Corporation). Unless otherwise noted, significance was evaluated using a two-tailed Student *t* test.

ACKNOWLEDGMENTS. We thank Dr. Shigeyuki Yokoyama (University of Tokyo) for the original pBpa vectors and for advice on pBpa incorporation and cross linking. We also thank Erik Soderblom, Meredith Turner, and Arthur Moseley (Duke University Proteomics Core Facility) for help with the MS analysis. This work was supported by National Institutes of Health Grants R21-CA-140030-01 and R01-NS059957 (to S.H.S.), Fonds National Suisse de la Recherche Scientifique Grant 3100A0-122020 (to D.D), and a grant from the Howard Hughes Medical Institute (to R.Y.).

- Schirmer EC, Florens L, Guan T, Yates JR, 3rd, Gerace L (2003) Nuclear membrane proteins with potential disease links found by subtractive proteomics. *Science* 301:1380–1382.
- Foster LJ, et al. (2006) A mammalian organelle map by protein correlation profiling. *Cell* 125:187–199.
- Blume-Jensen P, Hunter T (2001) Oncogenic kinase signalling. *Nature* 411:355–365.
- Rikova K, et al. (2007) Global survey of phosphotyrosine signaling identifies oncogenic kinases in lung cancer. *Cell* 131:1190–1203.
- Villén J, Beausoleil SA, Gerber SA, Gygi SP (2007) Large-scale phosphorylation analysis of mouse liver. *Proc Natl Acad Sci USA* 104:1488–1493.
- Choudhary C, Mann M (2010) Decoding signalling networks by mass spectrometry-based proteomics. *Nat Rev Mol Cell Biol* 11:427–439.
- Huttlin EL, et al. (2010) A tissue-specific atlas of mouse protein phosphorylation and expression. *Cell* 143:1174–1189.
- Mayer BJ, Jackson PK, Baltimore D (1991) The noncatalytic src homology region 2 segment of abl tyrosine kinase binds to tyrosine-phosphorylated cellular proteins with high affinity. *Proc Natl Acad Sci USA* 88:627–631.
- Marengere LE, Pawson T (1992) Identification of residues in GTPase-activating protein Src homology 2 domains that control binding to tyrosine phosphorylated growth factor receptors and p62. *J Biol Chem* 267:22779–22786.
- Bradshaw JM, Waksman G (2002) Molecular recognition by SH2 domains. *Adv Protein Chem* 61:161–210.
- Liu BA, et al. (2011) The SH2 domain-containing proteins in 21 species establish the provenance and scope of phosphotyrosine signaling in eukaryotes. *Sci Signal* 4:ra83.
- Blagoev B, et al. (2003) A proteomics strategy to elucidate functional protein-protein interactions applied to EGF signaling. *Nat Biotechnol* 21:315–318.
- Yang G, et al. (2009) Proteomic, functional and motif-based analysis of C-terminal Src kinase-interacting proteins. *Proteomics* 9:4944–4961.
- Okada H, et al. (2011) SH3 domain-based phototrapping in living cells reveals Rho family GAP signaling complexes. *Sci Signal* 4:rs13.
- Machida K, et al. (2007) High-throughput phosphotyrosine profiling using SH2 domains. *Mol Cell* 26:899–915.
- Overduin M, Rios CB, Mayer BJ, Baltimore D, Cowburn D (1992) Three-dimensional solution structure of the src homology 2 domain of c-abl. *Cell* 70:697–704.
- Zhu G, et al. (1994) Sequence specificity in the recognition of the epidermal growth factor receptor by the abl Src homology 2 domain. *Oncogene* 9:1379–1385.
- Mayer BJ, Hirai H, Sakai R (1995) Evidence that SH2 domains promote processive phosphorylation by protein-tyrosine kinases. *Curr Biol* 5:296–305.
- Moritz A, et al. (2010) Akt-RSK-56 kinase signaling networks activated by oncogenic receptor tyrosine kinases. *Sci Signal* 3:ra64.
- Liu BA, et al. (2010) SH2 domains recognize contextual peptide sequence information to determine selectivity. *Mol Cell Proteomics* 9:2391–2404.
- Huang H, et al. (2008) Defining the specificity space of the human SRC homology 2 domain. *Mol Cell Proteomics* 7:768–784.
- Sprang SR (2000) Conformational display: A role for switch polymorphism in the superfamily of regulatory GTPases. *Sci STKE* 2000:pe1.
- Vetter IR, Wittinghofer A (2001) The guanine nucleotide-binding switch in three dimensions. *Science* 294:1299–1304.
- Wei Y, et al. (1997) Crystal structure of RhoA-GDP and its functional implications. *Nat Struct Biol* 4:699–703.
- Yasuda R, et al. (2006) Supersensitive Ras activation in dendrites and spines revealed by two-photon fluorescence lifetime imaging. *Nat Neurosci* 9:283–291.
- Murakoshi H, Wang H, Yasuda R (2011) Local, persistent activation of Rho GTPases during plasticity of single dendritic spines. *Nature* 472:100–104.
- Chen Z, et al. (2010) Structure and control of the actin regulatory WAVE complex. *Nature* 468:533–538.
- Cuevas BD, et al. (2001) Tyrosine phosphorylation of p85 relieves its inhibitory activity on phosphatidylinositol 3-kinase. *J Biol Chem* 276:27455–27461.
- Feig LA, Cooper GM (1988) Relationship among guanine nucleotide exchange, GTP hydrolysis, and transforming potential of mutated ras proteins. *Mol Cell Biol* 8:2472–2478.
- Xu X, Barry DC, Settleman J, Schwartz MA, Bokoch GM (1994) Differing structural requirements for GTPase-activating protein responsiveness and NADPH oxidase activation by Rac. *J Biol Chem* 269:23569–23574.
- Longenecker K, et al. (2003) Structure of a constitutively activated RhoA mutant (Q63L) at 1.55 Å resolution. *Acta Crystallogr D Biol Crystallogr* 59:876–880.
- Kakiashvili E, et al. (2011) The epidermal growth factor receptor mediates tumor necrosis factor- α -induced activation of the ERK/GEF-H1/RhoA pathway in tubular epithelium. *J Biol Chem* 286:9268–9279.
- Lancaster CA, et al. (1994) Characterization of rhoGAP. A GTPase-activating protein for rho-related small GTPases. *J Biol Chem* 269:1137–1142.
- Zhou YT, Chew LL, Lin SC, Low BC (2010) The BNIP-2 and Cdc42GAP homology (BCH) domain of p50RhoGAP/Cdc42GAP sequesters RhoA from inactivation by the adjacent GTPase-activating protein domain. *Mol Biol Cell* 21:3232–3246.
- Tibaldi E, et al. (2008) Src-Tyrosine kinases are major agents in mitochondrial tyrosine phosphorylation. *J Cell Biochem* 104:840–849.
- Férelle E, et al. (1999) Insulin-induced stimulation of Na⁺/K⁺-ATPase activity in kidney proximal tubule cells depends on phosphorylation of the α -subunit at Tyr-10. *Mol Biol Cell* 10:2847–2859.
- Hantschel O, et al. (2005) Structural basis for the cytoskeletal association of Bcr-Abl/c-Abl. *Mol Cell* 19:461–473.
- Fincham VJ, Chudleigh A, Frame MC (1999) Regulation of p190 Rho-GAP by v-Src is linked to cytoskeletal disruption during transformation. *J Cell Sci* 112:947–956.
- Nozu F, Tsunoda Y, Ibitayo AI, Bitar KN, Owyang C (1999) Involvement of RhoA and its interaction with protein kinase C and Src in CCK-stimulated pancreatic acini. *Am J Physiol* 276:G915–G923.
- Arthur WT, Petch LA, Burridge K (2000) Integrin engagement suppresses RhoA activity via a c-Src-dependent mechanism. *Curr Biol* 10:719–722.
- Dvorsky R, Blumenstein L, Vetter IR, Ahmadian MR (2004) Structural insights into the interaction of ROCK1 with the switch regions of RhoA. *J Biol Chem* 279:7098–7104.
- Hutchinson CL, Lowe PN, McLaughlin SH, Mott HR, Owen D (2011) Mutational analysis reveals a single binding interface between RhoA and its effector, PRK1. *Biochemistry* 50:2860–2869.
- Kristelli R, Gao G, Tesmer JGG (2004) Structural determinants of RhoA binding and nucleotide exchange in leukemia-associated Rho guanine-nucleotide exchange factor. *J Biol Chem* 279:47352–47362.
- Li R, Zheng Y (1997) Residues of the Rho family GTPases Rho and Cdc42 that specify sensitivity to Dbp-like guanine nucleotide exchange factors. *J Biol Chem* 272:4671–4679.
- Worby CA, et al. (2009) The fic domain: Regulation of cell signaling by adenylation. *Mol Cell* 34:93–103.
- Guo A, et al. (2008) Signaling networks assembled by oncogenic EGFR and c-Met. *Proc Natl Acad Sci USA* 105:692–697.
- Tu S, Wu WJ, Wang J, Cerione RA (2003) Epidermal growth factor-dependent regulation of Cdc42 is mediated by the Src tyrosine kinase. *J Biol Chem* 278:49293–49300.
- Chang F, Lemmon C, Lietha D, Eck M, Romer L (2011) Tyrosine phosphorylation of Rac1: A role in regulation of cell spreading. *PLoS ONE* 6:e28587.
- Riedl J, et al. (2008) Lifeact: A versatile marker to visualize F-actin. *Nat Methods* 5:605–607.
- Skene JH, Virág I (1989) Posttranslational membrane attachment and dynamic fatty acylation of a neuronal growth cone protein, GAP-43. *J Cell Biol* 108:613–624.
- von Heijne G, Steppuhn J, Herrmann RG (1989) Domain structure of mitochondrial and chloroplast targeting peptides. *Eur J Biochem* 180:535–545.
- Durocher Y, Perret S, Kamen A (2002) High-level and high-throughput recombinant protein production by transient transfection of suspension-growing human 293-EBNA1 cells. *Nucleic Acids Res* 30:E9.
- Liu H, Sadygov RG, Yates JR, 3rd (2004) A model for random sampling and estimation of relative protein abundance in shotgun proteomics. *Anal Chem* 76:4193–4201.
- de Hoon MJL, Imoto S, Nolan J, Miyano S (2004) Open source clustering software. *Bioinformatics* 20:1453–1454.
- Saldanha AJ (2004) Java Treeview—Extensible visualization of microarray data. *Bioinformatics* 20:3246–3248.
- Soderling SH, et al. (2002) The WRP component of the WAVE-1 complex attenuates Rac-mediated signalling. *Nat Cell Biol* 4:970–975.
- Westphal RS, Soderling SH, Alto NM, Langeberg LK, Scott JD (2000) Scar/WAVE-1, a Wiskott-Aldrich syndrome protein, assembles an actin-associated multi-kinase scaffold. *EMBO J* 19:4589–4600.
- Mason FM, Heimsath EG, Higgs HN, Soderling SH (2011) Bi-modal regulation of a formin by srGAP2. *J Biol Chem* 286:6577–6586.

Supporting Information

Uezu et al. 10.1073/pnas.1207358109

SI Materials and Methods

Plasmids. Membrane-targeted phosphorylated enhanced yellow fluorescent protein (pEYFP and mitochondria-targeted pEYFP) were purchased from Clontech. GST-Src homology 2 (SH2) was made by subcloning into pGEX-4T vector (GE Healthcare). The following tyrosine kinase expression vectors were used: pLNCX-srcY527F (plasmid 13660; Addgene) and pBABEpuro-EGFRL858R (plasmid 32073; Addgene) (1), pcDNA-Bcr-Abl (gift of Brian Druker, Oregon Health Sciences University, Portland, OR), and Flag-tagged BrkY447F and ratHER2 (provided by Todd Miler, Stony Brook University, Stony Brook, NY, and H. Kim Lysterly, Duke University, respectively). Human RhoA coding sequence was cloned into pcDNA3-V5, pBetaActin-GFP, or pEGFP-C1 vector (Clontech). All V5 and GFP tags were added to the N terminus of RhoA. RhoA mutant constructs were made using the Site-Directed Mutagenesis Kit (Stratagene) according to the manufacturer's instructions. Plasmid containing mCherry-Rhotekin (8–89 amino acids)-mCherry was previously described (2). Constitutively active Src (srcY527F) or dominant negative Src (srcK295R, Y527F) was fused to the N terminus of mCherry-Rhotekin (8–89 amino acids)-mCherry with the modified 2A sequence (EGRGSLTTCGDVEENPGPAPGS) in between (3).

Tandem Affinity Purification. The cross-linked cell pellet was resuspended in 20 mL of tandem affinity purification (TAP) lysis buffer [50 mM Tris (pH 7.5), 150 mM NaCl, 1 mM EDTA, 7.5% (vol/vol) glycerol, 25 mM NaF, 0.5% Nonidet P-40, 1 mM Na₃VO₄, 1 mM DTT, 1 mM 4-(2-aminoethyl)benzenesulfonyl fluoride hydrochloride (AEBSF), 2 µg/mL leupeptin/pepstatin], homogenized with Dounce homogenizer, and subjected to centrifugation (17,000 × g) for 30 min. The supernatant was further clarified by ultracentrifugation (136,000 × g) for 1 h. The supernatant was mixed with IgG-Sepharose beads (200-µL bed volume) and incubated for 3 h at 4 °C. The beads were washed with TAP lysis buffer and 5 mL of tobacco etch virus (TEV) cleavage buffer [10 mM Tris (pH 7.5), 100 mM NaCl, 0.5 mM EDTA, 1% Triton X-100, 1 mM DTT, 1 mM AEBSF, 2 µg/mL leupeptin/pepstatin]. Beads were then resuspended with 0.2 mL of TEV cleavage buffer and incubated with TEV protease (100 units) and HRV3C protease (20 units; Accelagen) for 3 h at room temperature and overnight at 4 °C. The flow-through from the beads was mixed with calmodulin-Sepharose beads (400-µL bed volume) in 2× calmodulin binding peptide binding buffer [10 mM Tris (pH 7.5), 100 mM NaCl, 2 mM MgAc, 4 mM CaCl₂, 2 mM imidazole, 0.1% Nonidet P-40, 1 mM DTT, 1 mM AEBSF, 2 µg/mL leupeptin/pepstatin] and incubated for 2 h. After being washed with calmodulin-rinsing buffer [50 mM ammonium bicarbonate (pH 8.0), 75 mM NaCl, 1 mM MgAc, 2 mM CaCl₂, 1 mM imidazole, 1 mM AEBSF, 2 µg/mL leupeptin/pepstatin] and 50 mM ammonium bicarbonate, the column was incubated with calmodulin-elution buffer [50 mM ammonium bicarbonate (pH 8.0), 25 mM EGTA] containing 0.1% Rapigest for 10 min and eluted. Elution with calmodulin-elution buffer without Rapigest was repeated three more times. The eluates were combined and concentrated with an Amicon Ultra-4 (Millipore) at a 30,000 molecular weight cutoff.

Qualitative Identifications from Raw Liquid Chromatography/Tandem MS Data.

1. Yuza Y, et al. (2007) Allele-dependent variation in the relative cellular potency of distinct EGFR inhibitors. *Cancer Biol Ther* 6:661–667.
2. Murakoshi H, Wang H, Yasuda R (2011) Local, persistent activation of Rho GTPases during plasticity of single dendritic spines. *Nature* 472:100–104.

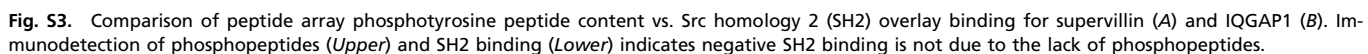
processed in Mascot distiller (Matrix Science) and then submitted to Mascot database searches (Matrix Science) against a UniProt database (*Homo sapiens* taxonomy) containing both forward and reverse entries of each protein. Search tolerances of 10-ppm precursor and 0.02-Da product ions were applied to all searches. All data were searched using trypsin specificity with up to two missed cleavages. Carbamidomethylation (+57.0214 Da on C) was set as a fixed modification, whereas oxidation (+15.9949 Da on M) was considered a variable modification.

Immunoprecipitation Experiments. Transfected cells were lysed with lysis buffer [25 mM Hepes (pH 7.4), 150 mM NaCl, 1 mM EDTA, 1% Nonidet P-40, 5 mM NaF, 1 mM orthovanadate, 1 mM AEBSF, 2 µg/mL leupeptin/pepstatin]. The lysate was centrifuged, and the supernatant was incubated with V5 antibody-agarose (Sigma) or GFP trap-agarose (ChromoTek). After beads were washed with lysis buffer, sample buffer was added and subjected to immunoblotting. For endogenous RhoA precipitation, cells were lysed with radio-immunoprecipitation assay buffer [20 mM Tris-HCl (pH 7.5), 150 mM NaCl, 1% EDTA, 0.1% SDS, 0.1% Triton X-100, 1% deoxycholate, 1 mM orthovanadate, protease inhibitors], followed by sonication and centrifugation, and the supernatant was incubated with agarose-conjugated anti-RhoA (26C4; Santa Cruz Biotechnology). Immunoprecipitated V5-tagged RhoA, tyrosine-phosphorylated proteins, or RhoA was detected by HRP-conjugated anti-V5 (Invitrogen), HRP-conjugated antiphosphotyrosine (Millipore), or anti-RhoA (67B9; Cell Signaling Technology) antibodies.

In Vitro Phosphorylation of GST-Fusion Proteins by Src. GST-fusion proteins (150 pmol) were incubated with 0.1 µg of purified Src (GenScript) in a kinase buffer [50 mM Hepes (pH 7.4), 10 mM MgCl₂, 1 mM DTT, 0.01% Triton X-100, 0.5 mM ATP] at 30 °C for 30 min. Reactions were terminated by the addition of SDS sample buffer.

Cell Preparation and Image Analysis. Transfected FreeStyle 293 cells were plated onto poly-D-lysine-coated coverslips for 1 h and fixed with 4% paraformaldehyde/4% sucrose in PBS for 15 min at 37 °C. After permeabilization with 0.1% Triton X-100 in PBS, cells were stained with anti-V5 antibody (1:500; Invitrogen) or antiphosphotyrosine antibody (1:100, 4G10; Millipore). Images were taken on a Zeiss LSM 710 laser scanning confocal microscope. All images were acquired using either a 63×/1.4 N.A. oil-immersion objective or a 20×/0.8 N.A. objective. For quantification of phalloidin staining, HeLa cells were transfected with V5-RhoA or their mutants using Lipofectamine 2000 (Invitrogen) for 12–18 h and serum-starved with 0.1% BSA in DMEM for 6 h. After fixation, cells were stained with V5 antibody and rhodamine-phalloidin (1:500; Invitrogen). To estimate the induction of F-actin formation, the average intensity of phalloidin or V5 staining per cell area was calculated, excluding the nucleus and the 5-µm edge from the border of the cell. First, the levels of F-actin in mock-transfected cells were quantified. Then, the levels of F-actin were quantified for each transfected cell expressing RhoA or RhoA mutant. The percentage of cells with F-actin levels above those of mock-transfected cells was quantified for each mutant and graphed. All images were taken using the same settings, and analysis was done with MetaMorph (version 7.7; Molecular Devices).

3. Tang W, et al. (2009) Faithful expression of multiple proteins via 2A-peptide self-processing: A versatile and reliable method for manipulating brain circuits. *J Neurosci* 29:8621–8629.



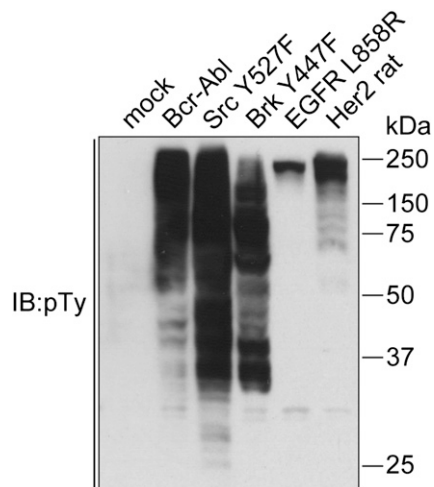


Fig. S4. Immunoblot (IB)-verifying activity for each tyrosine kinase mutant. Each tyrosine kinase (indicated above each lane) was expressed in 293T cells, and the cell lysates were blotted with antiphosphotyrosine antibody (pTy).

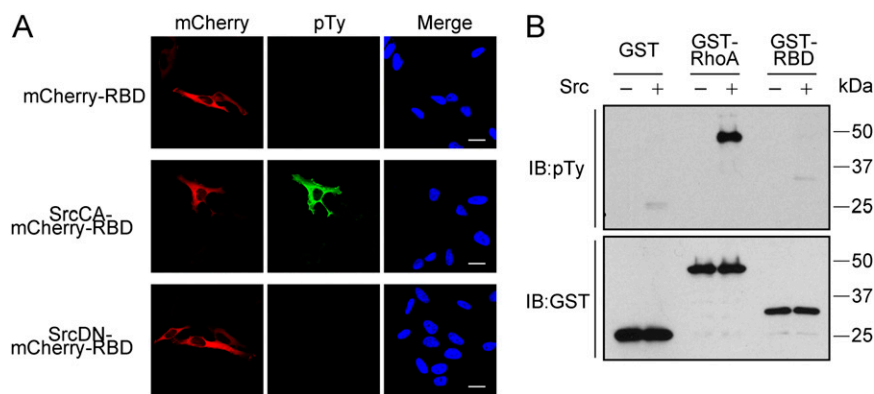


Fig. S5. (A) Coexpression and kinase activity of Src-2A-Rho binding domain (RBD) mutants. Coexpression of SrcCA (Y527F) and SrcDN (K295R and Y527F) with the acceptor, mCherry-RBD [mCherry-Rhotekin (8–89 amino acids)-mCherry], in HeLa cells is shown. Cells were fixed and stained with antiphosphotyrosine antibody (pTy; green) and DAPI (blue). (Scale bars, 20 μ m.) (B) Immunoblot (IB) of purified GST, GST-RhoA, or GST-RBD to detect phosphotyrosine after incubation with purified Src kinase (*Upper*) or input for each reaction (*Lower*).

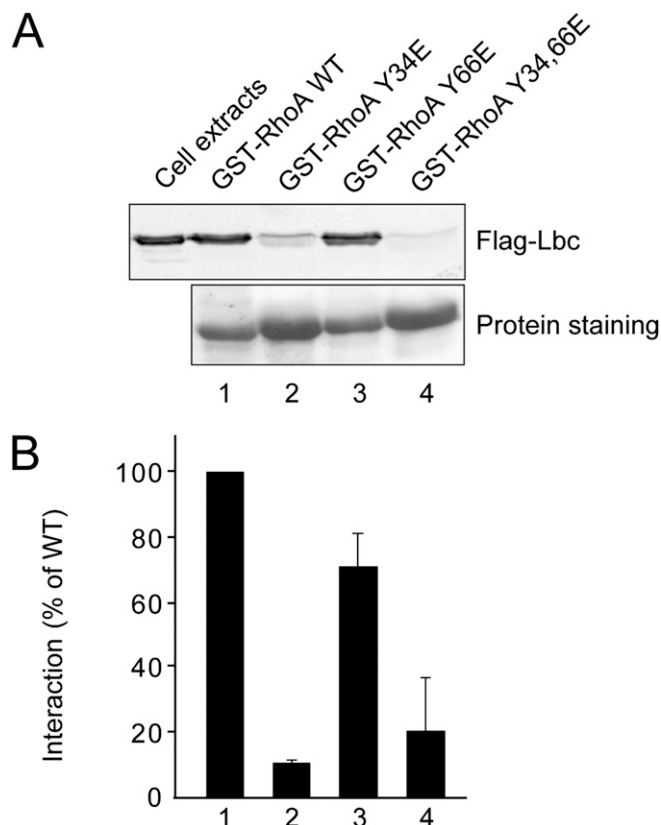


Fig. S6. Regulation of RhoA and Lbc binding by Y34 and Y66. (A) Lysates from 293T cells expressing Flag-tagged Lbc were incubated with GST-RhoA vs. RhoA phosphomimetic mutants. (Upper) Levels of Lbc bound to GST-RhoA or its mutants were determined by Western blot analysis after GST pull-downs. (Lower) Relative levels of each GST-RhoA fusion used in the pull-down assay are shown. (B) Graph depicts the quantification of the levels of associated RhoA or its mutants. Y34E reduces Lbc binding by 90%, whereas Y66E reduces binding by ~30%. Bars represent mean \pm SEM ($n = 4$).

Fig. S7. Sequence alignment of RhoA and its related small G-protein families around switch regions. Black dots indicate the tyrosine sites in RhoA. Tyrosine-phosphorylated residues (Y34 and Y66) revealed by this study are highlighted in red. Amino acids that are reported to be phosphorylated are highlighted by a red box (tyrosine) or circle (serine or threonine) for protein in the alignment. Alignment was constructed using Clustal Omega. The background color for amino acids corresponds to the conservation level (dark blue, well conserved; white, not conserved), as analyzed by Jalview version 2. UniProt accession numbers are as follows; RhoA P61586, RhoB P62745, RhoC P08134, Rac1 P63000, Cdc42 P40793, H-Ras P01112, Rap1A P62834, RalA P11233, Ran P62826, Arf6 P62330, Rab5A P20339, Rab11A P62491, and Rab4A P20338.

Dataset S1. List of proteins in each targeted Src homology 2 *p*-benzoyl-L-phenylalanine protein interaction cluster from hierarchical clustering of MS-identified proteins

[Dataset S1](#)

MS-identified proteins are described in Fig. 3A. Cellular localization was annotated by searching against the UniProt, AmiGO, and Human Protein Atlas databases. Reported phosphotyrosine sites are listed based on prior published data curated by means of the PhosphoSite and Phospho.ELM databases. n.S.C, normalized spectral count.

Dataset S2. Identification and quantification of phosphotyrosine-dependent Src homology 2 binding sites

[Dataset S2](#)

Peptides containing tyrosine sites from proteins in each subcellular targeted Src homology 2 (SH2) protein interaction cluster ([Dataset S1](#)) were synthesized onto cellulose membrane in nonphosphorylated and phosphorylated forms. Membranes were incubated with purified GST-SH2 domain and immunoblotted with anti-GST antibody. The peptide array immunoblots were densitometrically quantified. Binding strengths for each peptide were normalized to the control peptide derived from EGF receptor. Colored bars represent peptides previously reported to be tyrosine-phosphorylated.